J|A|C|S ARTICLES

Published on Web 05/29/2009

Exploring the Spatial Distribution and Transport Behavior of Charge Carriers in a Single Titania Nanowire

Takashi Tachikawa* and Tetsuro Majima*

The Institute of Scientific and Industrial Research (SANKEN), Osaka University, Mihogaoka 8-1, Ibaraki, Osaka 567-0047, Japan

Received January 9, 2009; E-mail: tachi45@sanken.osaka-u.ac.jp; majima@sanken.osaka-u.ac.jp

Abstract: One-dimensional nanostructures of metal oxide semiconductors have both potential and demonstrated applications for use in light waveguides, photodetectors, solar energy conversion, photocatalysis, etc. We investigated the transport and reaction dynamics of the photogenerated charge carriers in individual titania nanowires using single-particle photoluminescence (PL) spectroscopy. Examination of the spectral and kinetic characteristics revealed that the photoluminescence bands originating from defects in the bulk and/or on the surface appeared in the visible region with numerous photon bursts by photoirradiation using a 405-nm laser under an Ar atmosphere. From the single-molecule kinetic analysis of the bursts, it was found that the quenching reaction of trapped electrons by molecular oxygen follows a Langmuir−Hinshelwood mechanism. In addition, a novel spectroscopic method, i.e., single-molecule spectroelectrochemistry, was utilized to explore the nature of the defect states inherent in the wires. The spatially resolved PL imaging techniques thus enable us to ascertain the location of the luminescent active sites that are related to the heterogeneously distributed defects and to present experimental evidence of the long-distance transport of charge carriers in the wire. Consequently, this study provides a great opportunity to understand the role of defects in the behavior of charge carriers in TiO_2 nanomaterials with various morphologies.

Introduction

One-dimensional organic and inorganic nanostructures, such as nanorods, nanotubes, and nanowires, have been extensively investigated because they have both potential and demonstrated applications for use in light waveguides,[1,2] photodetectors,[1,3] solar energy conversion,[4,5] photocatalysis,[6] lithium batteries,[7] gas sensing,[8,9] etc. In particular, nanotubes and nanowires of metal oxides, such as SnO_2,[10] TiO_2,[5,11] and ZnO,[4,12,13] provide additional benefits in two main respects, compared to the commonly used nanoparticles: (i) the one-dimensional geometry facilitates rapid, long-distance electron transport to the electrodes, thereby helping to significantly increase the efficiency of devices, and (ii) due to their high length-to-diameter ratio and the total length reaching tens of micrometers, visible-light scattering and absorption are significantly enhanced in the nanostructures. Both effects have been verified in experiments.[14−20] For example, a recent study reported that the "effective" electron diffusion length, $L_n = (D_n\tau_n)^{1/2}$,[21] where D_n is the effective diffusion coefficient for the electron within the electrode and τ_n is the survival time of the electron with respect to recombination with the oxidized dye or regenerator, is on the order of 100 μm in titania nanotube cells, which is remarkably greater than that (about 10 μm) reported for typical dye-sensitized solar cells (DSSCs) constructed using nanocrystalline TiO_2 particles.[20]

(1) Wang, J.; Gudiksen, M. S.; Duan, X.; Cui, Y.; Lieber, C. M. *Science* **2001**, *293*, 1455–1457.
(2) Huang, M. H.; Mao, S.; Feick, H.; Yan, H.; Wu, Y.; Kind, H.; Weber, E.; Russo, R.; Yang, P. *Science* **2001**, *292*, 1897–1899.
(3) Kind, H.; Yan, H.; Messer, B.; Law, M.; Yang, P. *Adv. Mater.* **2002**, *14*, 158–160.
(4) Law, M.; Greene, L. E.; Johnson, J. C.; Saykally, R.; Yang, P. *Nat. Mater.* **2005**, *4*, 455–459.
(5) Mor, G. K.; Varghese, O. K.; Paulose, M.; Shankar, K.; Grimes, C. A. *Sol. Energy Mater. Sol. Cells* **2006**, *90*, 2011–2075.
(6) Chen, X.; Mao, S. S. *Chem. Rev.* **2007**, *107*, 2891–2959.
(7) Bruce, P. G.; Scrosati, B.; Tarascon, J.-M. *Angew. Chem., Int. Ed.* **2008**, *47*, 2930–2946.
(8) Wang, Y.; Jiang, X.; Xia, Y. *J. Am. Chem. Soc.* **2003**, *125*, 16176–16177.
(9) McAlpine, M. C.; Ahmad, H.; Wang, D.; Heath, J. R. *Nat. Mater.* **2007**, *6*, 379–384.
(10) Gubbala, S.; Chakrapani, V.; Kumar, V.; Sunkara, M. K. *Adv. Funct. Mater.* **2008**, *18*, 2411–2418.
(11) Bavykin, D. V.; Friedrich, J. M.; Walsh, F. C. *Adv. Mater.* **2006**, *18*, 2807–2824.
(12) Leschkies, K. S.; Divakar, R.; Basu, J.; Enache-Pommer, E.; Boercker, J. E.; Carter, C. B.; Kortshagen, U. R.; Norris, D. J.; Aydil, E. S. *Nano Lett.* **2007**, *7*, 1793–1798.
(13) Martinson, A. B. F.; Elam, J. W.; Hupp, J. T.; Pellin, M. J. *Nano Lett.* **2007**, *7*, 2183–2187.
(14) Martinson, A. B. F.; McGarrah, J. E.; Parpia, M. O. K.; Hupp, J. T. *Phys. Chem. Chem. Phys.* **2006**, *8*, 4655–4659.
(15) Enache-Pommer, E.; Boercker, J. E.; Aydil, E. S. *Appl. Phys. Lett.* **2007**, *91*, 123116/1–123116/3.
(16) Ohsaki, Y.; Masaki, N.; Kitamura, T.; Wada, Y.; Okamoto, T.; Sekino, T.; Niihara, K.; Yanagida, S. *Phys. Chem. Chem. Phys.* **2005**, *7*, 4157–4163.
(17) Zhu, K.; Vinzant, T. B.; Neale, N. R.; Frank, A. J. *Nano Lett.* **2007**, *7*, 3739–3746.
(18) Tachikawa, T.; Tojo, S.; Fujitsuka, M.; Sekino, T.; Majima, T. *J. Phys. Chem. B* **2006**, *110*, 14055–14059.
(19) Zhu, K.; Neale, N. R.; Miedaner, A.; Frank, A. J. *Nano Lett.* **2007**, *7*, 69–74.
(20) Jennings, J. R.; Ghicov, A.; Peter, L. M.; Schmuki, P.; Walker, A. B. *J. Am. Chem. Soc.* **2008**, *130*, 13364–13372.
(21) Bisquert, J. *J. Phys. Chem. B* **2004**, *108*, 2323–2332.

Previously, a number of studies have been performed to clarify the dynamics of the transport, trapping, and recombination of charge carriers generated in DSSCs by various techniques, such as intensity-modulated photocurrent and photovoltage spectroscopies,[22−24] transient photocurrent and photovoltage,[22,25−27] and transient microwave conductivity and absorption techniques.[28,29] However, it is extremely difficult or impossible to distinguish between the above-mentioned effects in dense arrays of nanotubes or nanowires and ti elucidate the influence of the structural disorders, such as defects and size and shape non-uniformities, on the spatial distribution and transport properties of charge carriers using conventional ensemble measurements. Furthermore, in situ observations of the interfacial electron-transfer reactions on individual nanostructures provide a means of exploring the photocatalytically active sites heterogeneously distributed over the materials. Therefore, future techniques for examining a single piece of material are definitely required for designing and synthesizing efficient devices and photocatalysts.[30,31]

Herein, for the first time, we investigated the transport and reaction dynamics of the photogenerated charge carriers in individual TiO_2−B nanowires (noted as TNWs; structural and optical characterization of TNWs is given in the Supporting Information, Figures S1−4) using single-particle photoluminescence (PL) spectroscopy. TiO_2−B is an n-type semiconductor with a band gap of 3.0−3.2 eV,[32] which is similar to rutile and anatase, and has the advantage over the other polymorphs of being a relatively open structure.[33]

We have recently clarified the mechanism of the defect-mediated PL dynamics of TiO_2 nanoparticles at the single-particle or aggregate level.[34] The quantitative examination of the spectral and kinetic characteristics revealed that the PL bands originating from defects in the bulk and/or on the surface appeared in the visible region with numerous photon bursts by the photoirradiation with a 405-nm laser in an inert gas atmosphere. For the individual TNWs, similar PL behaviors were observed. In addition, a novel spectroscopic method, i.e., single-molecule spectroelectrochemistry,[35,36] is utilized to explore the nature of the luminescent defects present in the wire. This method is a powerful new technique for studying electrochemical kinetics in highly heterogeneous systems and allows us to measure electrochemical kinetics of many individual materials at a time. Moreover, the spatially resolved single-particle PL imaging techniques make it possible both to ascertain the spatial distribution of the luminescent active sites that are possibly related to the intrinsic defects and to obtain experimental evidence of the long-distance transport of charge carriers in the wire. Consequently, the present study offers a significant opportunity to understand the role of defects in the behavior of charge carriers in TiO_2 nanomaterials with various morphologies.

Experimental Section

Materials. TiO_2−B nanowires were synthesized in a high yield by a simple hydrothermal reaction as described elsewhere.[32,33,37] In a typical procedure, an aqueous suspension of 10 M NaOH and TiO_2 powder (P25, Nippon Aerosil) was stirred for 1 h and heated in a Teflon-lined stainless steel autoclave at 180 °C for 72 h. The resulting material was filtered, washed with a 0.1 M HCl solution and Milli-Q water to pH 7, and then dried at 90 °C for 12 h. The TiO_2−B nanowires were prepared by heating the washed titanate nanowires at 400 °C for 3 h in air. The details of the morphology (SEM, TEM, and AFM images), crystal structure (powder XRD pattern), and optical property (steady-state UV−visible diffuse reflectance and emission spectra) of the synthesized TNWs are given in the Supporting Information (Figures S1−4).

Sample Preparation. For the single-particle PL measurements, the cover glasses (22 × 22 mm^2) were purchased from Matsunami Glass and cleaned by sonication in a 20% detergent solution (As One, Cleanace) for 6 h, followed by repeated washing with running water for 30 min. Finally, the cover glasses were washed with Milli-Q water. An aqueous suspension of the TNW (2 mg mL^{-1}, pH 3, HNO_3(aq), 40 μL) was cast on the clean cover glass by spin-coating at 2000 rpm for 50 s, followed by annealing the TNWs-coated cover glass at 90 °C for 1 h in order for the wires on the glass not to peel off during the immersion in the solution. After the annealing, the TNWs-immobilized cover glass was repeatedly washed with Milli-Q water and dried in an inert gas. The sample was enclosed in a homemade glovebox, and the oxygen concentration inside the box was adjusted by an Ar gas purge. The relative humidity was maintained between 20 and 30% during the measurements. The relative humidity and oxygen concentration were measured by a Thermo-Hydrometer (As One) and Oxygen Analyzer, maxO_2+ (Maxtec, Inc.), respectively.

Single-Particle PL Measurements. The experimental setup for single-particle PL measurements is based on an Olympus IX71 inverted fluorescence microscope. A linearly or circularly polarized light emitted from a 405-nm CW diode laser (Olympus, LD405, 0.5 kW cm^{-2}) that passed through an objective lens (Olympus, UPlanSApo, 1.40 NA, 100×) after the reflection at a dichroic mirror (Olympus, DM455) was used to excite the wire. The polarization was controlled by a polarizer and a quarter- or a half-wave plate. The emission from TNWs on the cover glass was collected using an oil-immersion microscope objective, magnified by the built-in 1.6× magnification changer (thus, net magnification is 160×), passed through an emission filter (Olympus, BA475) to remove the undesired scattered light, and imaged by an electron-multiplying charge-coupled device (EM-CCD) camera (Roper Scientific, Cascade II:512). The images were recorded at 5−20 frames s^{-1} and processed using Image-Pro Plus software (Roper Scientific, ver. 6.2) and ImageJ software (http://rsb.info.nih.gov/ij/).

For the spectroscopy, only the emission that passed through a slit entered the imaging spectrograph (Acton Research, SP-2356) equipped with an EM-CCD camera (Princeton Instruments, PhotonMAX:512B). The width of the slit was 200 μm, which

(22) Cao, F.; Oskam, G.; Meyer, G. J.; Searson, P. C. *J. Phys. Chem.* **1996**, *100*, 17021–17027.
(23) Schlichthoerl, G.; Huang, S. Y.; Sprague, J.; Frank, A. J. *J. Phys. Chem. B* **1997**, *101*, 8141–8155.
(24) Fisher, A. C.; Peter, L. M.; Ponomarev, E. A.; Walker, A. B.; Wijayantha, K. G. U. *J. Phys. Chem. B* **2000**, *104*, 949–958.
(25) Solbrand, A.; Lindstroem, H.; Rensmo, H.; Hagfeldt, A.; Lindquist, S.-E.; Soedergren, S. *J. Phys. Chem. B* **1997**, *101*, 2514–2518.
(26) Duzhko, V.; Timoshenko, V. Y.; Koch, F.; Dittrich, T. *Phys. Rev. B* **2001**, *64*, 075204/1–075204/7.
(27) Timoshenko, V. Y.; Duzhko, V.; Dittrich, T. *Phys. Status Solidi A* **2000**, *182*, 227–232.
(28) Kroeze, J. E.; Savenije, T. J.; Warman, J. M. *J. Am. Chem. Soc.* **2004**, *126*, 7608–7618.
(29) Haque, S. A.; Tachibana, Y.; Willis, R. L.; Moser, J. E.; Grätzel, M.; Klug, D. R.; Durrant, J. R. *J. Phys. Chem. B* **2000**, *104*, 538–547.
(30) Roeffaers, M. B. J.; Sels, B. F.; Uji-i, H.; De Schryver, F. C.; Jacobs, P. A.; De Vos, D. E.; Hofkens, J. *Nature* **2006**, *439*, 572–575.
(31) Akimov, A. V.; Mukherjee, A.; Yu, C. L.; Chang, D. E.; Zibrov, A. S.; Hemmer, P. R.; Park, H.; Lukin, M. D. *Nature* **2007**, *450*, 402–406.
(32) Wang, G.; Wang, Q.; Lu, W.; Li, J. *J. Phys. Chem. B* **2006**, *110*, 22029–22034.
(33) Armstrong, A. R.; Armstrong, G.; Canales, J.; Bruce, P. G. *Angew. Chem., Int. Ed.* **2004**, *43*, 2286–2288.
(34) Tachikawa, T.; Ishigaki, T.; Li, J.-G.; Fujitsuka, M.; Majima, T. *Angew. Chem., Int. Ed.* **2008**, *47*, 5348–5352.
(35) Palacios, R. E.; Fan, F.-R. F.; Bard, A. J.; Barbara, P. F. *J. Am. Chem. Soc.* **2006**, *128*, 9028–9029.
(36) Palacios, R. E.; Fan, F.-R. F.; Grey, J. K.; Suk, J.; Bard, A. J.; Barbara, P. F. *Nat. Mater.* **2007**, *6*, 680–685.
(37) Daoud, W. A.; Pang, G. K. H. *J. Phys. Chem. B* **2006**, *110*, 25746–25750.

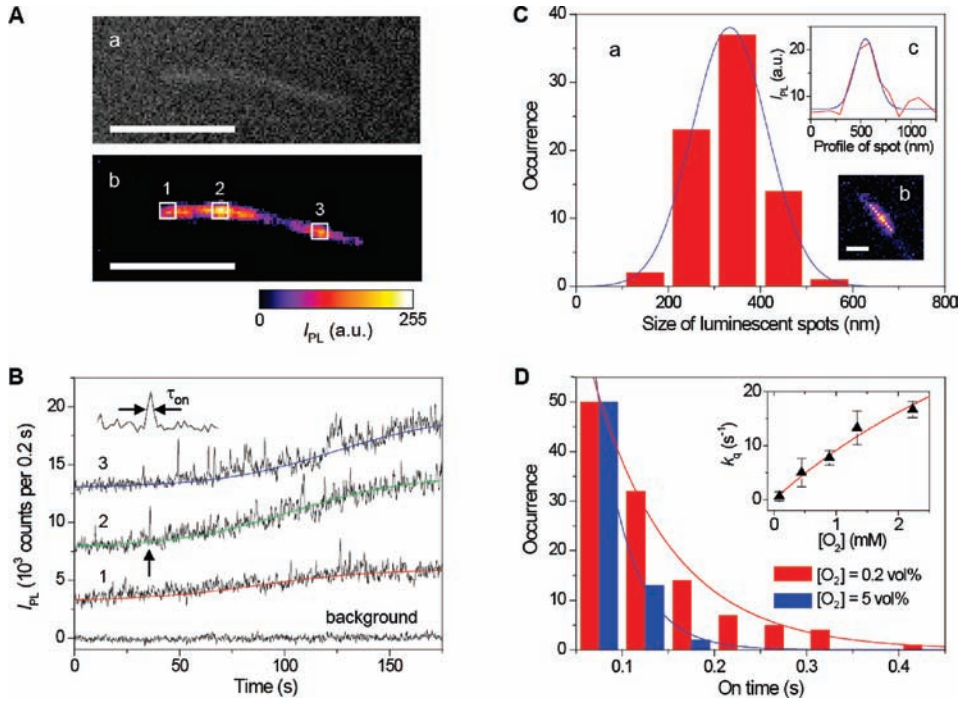

Figure 1. (A) Typical PL images observed for a single TNW on the glass surface under the 405-nm laser irradiation for 3 min in ambient air (a) and Ar (b). Scale bars are 5 μm. In image a, the emission mostly comes from scattered light. (B) Trajectories of the PL intensity (I_{PL}) obtained for the corresponding positions on a single TNW shown in image b of panel A (black lines). The background signal is also shown. The solid color lines indicate the kinetic traces calculated by eq 2. The trajectories observed for the different positions are well reproduced using the same parameter set for k^+ and k^-. See the text for details. The arrow indicates the photon burst (see also the inset in the figure). No significant decrease of the PL intensity and no detectable morphological change were observed for individual wires during the photoirradiation. (C) Histogram of the size of the burst-like luminescent spots (see image b) calculated from the width of the Gaussian distribution (red bars). The scale bar in image b is 1 μm. The blue line indicates the Gaussian distribution fitted with the histogram. The line profile of each burst is well fitted by a Gaussian distribution (c). (D) Histogram of "on" time (τ_{on}) determined for the bursts under oxygen concentrations of 0.2 (red) and 5 (blue) vol %. The integration time per one frame was 50 ms. The solid lines indicate the single-exponential fits. Inset shows the oxygen concentration dependence of the average quenching rate constant (k_q), which is calculated from $1/\tau_{on} - 1/\tau_{on}^0$, where τ_{on} and τ_{on}^0 are the "on" times of the bursts in the presence and absence of oxygen, respectively. The red line is obtained from eq 4, and the fitting parameters are as follows: $K_{ad} = 150$ M^{-1} and $[O_2]_{bs} = 68$ M. See text and the Supporting Information for details.

corresponds to 1.25 μm at the specimen, because the images at the slit were magnified by 160×. The spectra were typically integrated for 5 s. The spectrum detected by the EM-CCD camera was stored and analyzed using a personal computer. All the experimental data were obtained at room temperature.

Single-Particle Electrochemical Measurements. The single-particle electrochemical measurements were carried out at room temperature using an electrochemical analyzer (ALS, model 660A) with a standard three-electrode configuration. The working electrode (WE) was prepared by spin-casting aqueous suspensions of TNWs on a cleaned, ITO-coated cover glass (100 nm thickness, 10 Ω cm^{-2}, 80% transmittance at 405 nm, Matsunami Glass). The cell configuration is analogous to that reported by Barbara and co-workers, as illustrated in Figure S5 (Supporting Information).[35,36] The counter electrode (CE) was made by thermal-evaporating consecutive thin layers of chromium (15 nm) and gold (70 nm) over a cleaned cover glass using a homemade mask. Two homemade silicone spacers were used to hold the silver wire quasi-reference electrode (QRE) and to create a chamber between the WE and QRE which was filled with the Ar-purged 0.1 M $LiClO_4$ acetonitrile solution. Electrical connections to the three electrodes were made using silver paint and copper wires. The silver wire QRE potentials were observed to be about 0.22 V more negative than a ferrocenium/ferrocene (Fc/Fc^+) couple internal standard that was introduced into the cell after the single-particle electrochemical data were acquired. The reported potentials herein are relative to QRE.

Results and Discussion

Photoactivated PL of Single TNWs. Individual TNWs show a very weak emission in the visible region, which mostly comes from scattered light during 405-nm laser irradiation in ambient air, as shown in image a of Figure 1A. However, a dramatic increase in the emission intensity was observed by changing the atmosphere from air to Ar during the photoirradiation. A similar enhancement in the PL intensity was previously reported for TiO_2 nanoparticles, and this phenomenon was interpreted in terms of the defect-mediated photoactivation process.[34] The spectral measurements on single wires as well as bulk samples clearly show the growth of a very broad PL band in the visible region (475−750 nm, see Figure S4, Supporting Information), which originated from various defects associated with oxygen vacancies in the TiO_2 (so-called "color centers"),[38,39] as discussed below.

Photoactivation of the TNW PL, i.e., an order of magnitude or more increase in intensity, seems to be similar to that frequently observed for luminescent nanocolloids, such as CdSe and CdTe quantum dots,[40−44] but their mechanisms are completely different from each other. In the present system, light

(38) Serpone, N. *J. Phys. Chem. B* **2006**, *110*, 24287–24293.
(39) Kuznetsov, V. N.; Serpone, N. *J. Phys. Chem. C* **2007**, *111*, 15277–15288.
(40) Cordero, S. R.; Carson, P. J.; Estabrook, R. A.; Strouse, G. F.; Buratto, S. K. *J. Phys. Chem. B* **2000**, *104*, 12137–12142.
(41) Wang, Y.; Tang, Z.; Correa-Duarte, M. A.; Liz-Marzan, L. M.; Kotov, N. A. *J. Am. Chem. Soc.* **2003**, *125*, 2830–2831.
(42) Javier, A.; Strouse, G. F. *Chem. Phys. Lett.* **2004**, *391*, 60–63.
(43) Uematsu, T.; Maenosono, S.; Yamaguchi, Y. *J. Phys. Chem. B* **2005**, *109*, 8613–8618.
(44) Lee, S. F.; Osborne, M. A. *J. Am. Chem. Soc.* **2007**, *129*, 8936–8937.

Scheme 1. Reaction Schemes for the Photoactivation Processes[a]

$$TiO_2 + h\nu\ (405\ nm) \rightarrow e^-_{free} + h^+_{free}$$

(intrinsic absorption)

$$e^-_{free} \rightarrow e^-_{tr}\ (color\ centers)$$

$$h^+_{free} \rightarrow h^+_{tr}$$

$$e^-_{tr}\ (color\ centers) + h\nu\ (405\ nm) \rightarrow e^-_{free} + h^+_{free}$$

(extrinsic absorption)

$$e^-_{free} + h^+_{free/tr} \rightarrow PL$$

$$e^-_{tr}\ (color\ centers) + h^+_{free/tr} \rightarrow PL$$

$$e^-_{free} + O_2 \rightarrow O_2^{\bullet -}$$

[a] Visible color centers, most probably trapped electrons (e^-_{tr}) in the vacancy defect sites, are generated by the intrinsic and/or extrinsic excitations of TNWs under the 405-nm laser irradiation. Both e^-_{free} and e^-_{tr} can then recombine with the photogenerated holes ($h^+_{free/tr}$) to produce the PL in the UV and visible regions, respectively. In our experimental setup, only the latter could be detected. The quenching of e^-_{free} by O_2 molecules consequently results in the decreased PL. Based on the schemes, the main feature of the kinetics during visible-light irradiation is described as the dependence of the absorbance of the sample on the number of color centers (N). See ref 39 for a precise formulation.

absorption in the spectral region of the intrinsic absorption ($h\nu > 3.1 \pm 0.1$ eV) and in the bands corresponding to the color centers (extrinsic absorption, $h\nu < 3.1 \pm 0.1$ eV) generates free carriers that induce the formation of trapped carriers and surface oxygen species, such as the superoxide radical anion ($O_2^{\bullet -}$), which oxidize the color centers (Figure S4, Supporting Information).[34]

According to the literature,[39] the main feature of the kinetics during visible-light irradiation is the dependence of the absorbance of the sample on the number of color centers (N) (Scheme 1).

The differential equation for the formation (k^+) and deactivation (k^-) rates of the color centers is simply given by

$$\frac{dN}{dt} = k^+N - k^-N^2 \qquad (1)$$

The k^+ value depends on the light intensity, the absorbance of the color centers, and the quantum yield of the photoreaction. On the other hand, k^- depends on these same factors in addition to the oxygen content available in the gas-phase environment. Equation 1 is of the form of the Bernoulli equation and is converted into a first-order linear differential equation as given by

$$N(t) = \frac{1}{\frac{k^-}{k^+} - \left(\frac{k^-}{k^+} - \frac{1}{N_0}\right)\exp(-k^+t)} \qquad (2)$$

where N_0 is the number of color centers that exist prior to irradiation. The observed trajectories of the PL intensity were well reproduced by eq 2.[45] Although it is difficult to estimate the absolute value, the N values increased by at least 20 times after the photoactivation. This contains information difficult or impossible to obtain from ensemble experiments since each wire and position behave differently (Figure S6, Supporting Information). Assuming that the absorption cross section and PL quantum yield of the color centers are constant,[34] the k^+ and k^- values are determined on the basis of eq 2. Interestingly, the trajectories observed for the different positions on a wire were well reproduced by changing the N_0 values (0.0030, 0.0018, and 0.0009 au for positions 1, 2, and 3 in image b of Figure 1A, respectively) on the fixed parameter set for k^+ (0.04 s^{-1}) and k^- (0.50 s^{-1}).[46] The difference in N_0 at each position is possibly due to the heterogeneous distribution of defects inherent in the individual TNWs. The determined k^+ and k^- are similar to those (0.05 s^{-1} for k^+ and 0.50 s^{-1} for k^-) obtained for anatase TiO_2 nanoparticles under the same experimental conditions,[34] implying that the nature of related defect states is not very different, whereas the number of inherent defects is very different between them. This is not surprising because TiO_2−B and anatase are structurally related in that they have chains of edge-sharing octahedra in one orientation while the other polymorphs, such as rutile and brookite, have chains in two orientations.[47,48] The independence of the emission intensity of the randomly oriented TNWs on the (parallel and perpendicular) polarization of incident light also suggests that the increased PL is due to the heterogeneously distributed defects (data not shown).

Additionally, it should be noted that the photoactivation was accompanied by numerous "photon bursts" and their frequency of appearance gradually increased until saturation of the PL intensity occurred (for example, see the black arrow in Figure 1B, the inset, and Movie S1, Supporting Information). Image b of Figure 1C shows a typical burst-like luminescent spot acquired at 50 ms $frame^{-1}$ under an Ar atmosphere ($[O_2] = 0.2$ vol %). The cross sections of the individual spots have a full width at half-maximum of about 300 nm, which is very close to the theoretical diffraction limit of the optical microscope.

It appears that a large number of color centers formed in the bulk and/or on the surface are deactivated with a characteristic lifetime. The most direct way to evaluate the burst behavior is to record the emission intensity as a function of time, to distinguish between the "on" times (τ_{on}) and background signals by means of a threshold chosen to be 3σ greater than the noise levels, and to measure the distribution of τ_{on} as a histogram. As shown in Figure 1D, most of the bursts disappeared within

(45) Both intrinsic and extrinsic absorption of 405-nm light by TiO_2 and the color centers might activate a competitive process of formation and destruction of the color centers associated with oxygen vacancies.[39] However, considering the fact that TNW has a low intrinsic absorption at 405 nm, extrinsic transitions due to the color centers should be preferentially excited during the photoactivation process. Therefore, for ease of analysis, only eq 2 derived for the extrinsic absorption was employed in this study.

(46) The determined rate constants are several orders of magnitude faster than those reported in ref 39. This is mainly due to the higher light intensity used in this study.

(47) Banfield, J. F.; Veblen, D. R. *Am. Mineral.* **1992**, *77*, 545–557.
(48) Feist, T. P.; Davies, P. K. *J. Solid State Chem.* **1992**, *101*, 275–295.

(49) According to the literature,[50,52] the power law distribution indicates the existence of a wide distribution for both "on" and "off" times in the fluorescence intensity traces of single luminescent nanomaterials, such as CdSe quantum dots and wires. A similar analytical approach was applied to our data. We fitted the "on" time probability density, $P_{on}(t)$, obtained for single TNWs in Ar ($[O_2] = 0.2$ vol %) to a power law, $P_{on}(t) = At^{-\alpha_{on}}$, where A is the scaling coefficient and α_{on} is the power law exponent. The α_{on} value was determined to be 2.5 ± 0.1 ($R^2 = 0.95$), which is much higher than those (1.7−1.9) reported for the single quantum dots and wires of CdSe.[50,52] It was also found that the $P_{on}(t)$ is well fitted by a single-exponential decay function ($R^2 = 0.99$). These results imply that the intrinsic physical mechanism originates from an exponential decay dynamics associated with a single Poisson distribution. See Figure S7 (Supporting Information).

a few hundred milliseconds under an Ar atmosphere ([O_2] = 0.2 vol %).[49] The possible explanations for the limited lifetime of the bursts are as follows: (i) the charge recombination of the color centers with the photogenerated holes, (ii) the scavenging of the color centers by residual oxygen molecules or adventitious impurities, and (iii) photostimulated detrapping of the color centers to give mobile electrons.[53] In order to elucidate the mechanism of the burst-like PL phenomenon, the oxygen concentration dependence was examined. The experimental and analytical results in Figure 1D indeed demonstrate a significant decrease in τ_{on} from 85 ± 6 to 36 ± 2 ms, which are derived by a single-exponential fitting, by increasing the oxygen concentration to 5 vol %. The frequency of the burst generation rapidly decreased with increasing oxygen concentration ([O_2] > 5 vol %), and eventually only one or no counts during the course of the experiment (15 s) were observed in an air atmosphere ([O_2] = 21 vol %). These observations are indicative of a second-order reaction between electrons and oxygen molecules and a saturation of available oxygen binding sites on the surface of the wire.

We now consider in more detail the quenching dynamics of the photon bursts in accordance with the Langmuir−Hinshelwood equation which is successfully used to explain the photocatalytic reduction of oxygen molecules adsorbed on the nanocrystalline TiO_2 films.[54]

According to the model, the average quenching rate of the bursts by oxygen is described by

$$k_q = k_q^0[O_2]_{ad} = \frac{1}{\tau_{on}} - \frac{1}{\tau_{on}^0} \quad (3)$$

where k_q^0 is the second-order reaction rate constant for electron transfer, $[O_2]_{ad}$ is the concentration of adsorbed oxygen molecules on the TiO_2 surface, and τ_{on}^0 is the "on" time of the bursts in the absence of oxygen. The τ_{on}^0 value was estimated to be 91 ± 6 ms from the intercept of the plots of τ_{on}^{-1} versus the concentration of oxygen in the gas phase (Figure S8, Supporting Information). As shown in the inset of Figure 1D, the plots of k_q as a function of the oxygen concentration in the gas phase can be fitted by a simple Langmuir adsorption isotherm,[54]

$$[O_2]_{ad} = \frac{K_{ad}[O_2][O_2]_{bs}}{1 + K_{ad}[O_2]} \quad (4)$$

where K_{ad} is the equilibrium adsorption constant for the oxygen binding and $[O_2]_{bs}$ is the concentration of the oxygen binding sites. Based on this equation, we obtained the K_{ad} value of 150 ± 50 M^{-1} which is on the same order as those reported elsewhere.[54,55] Moreover, the quenching yield of the bursts by oxygen, which is defined as $\phi_q = 1 - (\tau_{on}/\tau_{on}^0)$, increased to ca. 60% as the oxygen concentration increased to 5 vol % (Figure S8, Supporting Information). It should be noted here that the electron half-times in the nanocrystalline TiO_2 film are reported to be about 60 and 550 ms in the presence (5 vol %) and absence of oxygen, respectively.[54] Comparison with our single-molecule analysis data enables us to deduce that τ_{on} is explained not only by the scavenging of the mobile electrons by oxygen molecules but also by other factors. At the present stage, we consider that the bursts originated from the radiative recombination of holes and electrons at the color centers, such as the oxygen vacancies (V_O) with one or two trapped electrons, i.e., the F^+ or F center.[38,56] To fully understand the burst phenomenon, however, the temperature and laser power effects on the luminescence characteristics must be examined. We hope to carry out such measurements in the near future.

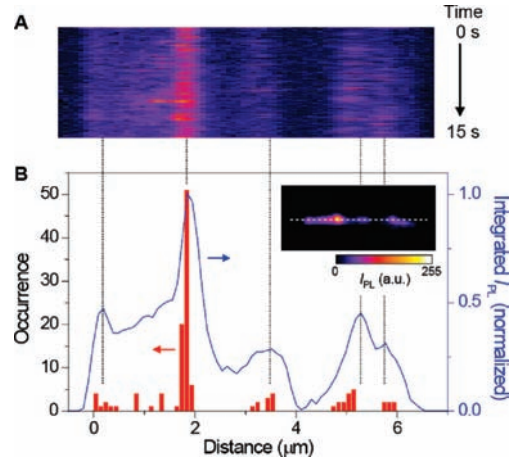

Figure 2. (A) Time course of the emission intensity profile along the broken line shown in the image of panel B. (B) Histogram of the number of counted bursts (red) and the line profile of the integrated PL intensity over 15 s during the photoactivation process (blue). The precise position at which a burst is generated is determined from Gaussian fits to the intensity profiles.

Spatial Distribution of Light-Emitting Color Centers. In Figure 2, we show the time course of the emission intensity profile along the broken line in the image of Figure 2B and the histogram for the number of counted bursts (red bars). In this case, the precise position at which a burst is generated is determined from the Gaussian fits to the intensity profiles. For the sake of comparison, the line profile of the integrated PL intensity over 15 s during the photoactivation process is also shown by the blue line in Figure 2B. The location of the burst generation approximately corresponds to the peaks in the profile, suggesting that the burst phenomenon is closely related to the photoactivation process, and the luminescent active sites, which are possibly attributed to the intrinsic distribution of defects, are heterogeneously distributed over the wire. Although no information about the absolute number of defects present in individual TNWs could be extracted from the present data, the active sites capable of detecting the bursts are roughly estimated to be 2−5 sites/μm for 20 individual wires. These active sites would be closely related to structural disorders, such as cracks and kinks, and the heterogeneous distribution of the surface states present in the individual wires.[57]

Time Evolution of PL Spectra. Photoactivation of the TNWs also accompanies the dramatic spectral change. Figure 3 shows

(50) Kuno, M.; Fromm, D. P.; Hamann, H. F.; Gallagher, A.; Nesbitt, D. J. *J. Chem. Phys.* **2001**, *115*, 1028–1040.
(51) Protasenko, V. V.; Hull, K. L.; Kuno, M. *Adv. Mater.* **2005**, *17*, 2942–2949.
(52) Glennon, J. J.; Tang, R.; Buhro, W. E.; Loomis, R. A. *Nano Lett.* **2007**, *7*, 3290–3295.
(53) Shkrob, I. A.; Sauer, M. C., Jr. *J. Phys. Chem. B* **2004**, *108*, 12497–12511.
(54) Peiro, A. M.; Colombo, C.; Doyle, G.; Nelson, J.; Mills, A.; Durrant, J. R. *J. Phys. Chem. B* **2006**, *110*, 23255–23263.
(55) Addamo, M.; Augugliaro, V.; Coluccia, S.; Faga, M. G.; García-López, E.; Loddo, V.; Marcì, G.; Martra, G.; Palmisano, L. *J. Catal.* **2005**, *235*, 209–220.
(56) Lei, Y.; Zhang, L. D.; Meng, G. W.; Li, G. H.; Zhang, X. Y.; Liang, C. H.; Chen, W.; Wang, S. X. *Appl. Phys. Lett.* **2001**, *78*, 1125–1127.
(57) Johnson, J. C.; Yan, H.; Yang, P.; Saykally, R. J. *J. Phys. Chem. B* **2003**, *107*, 8816–8828.

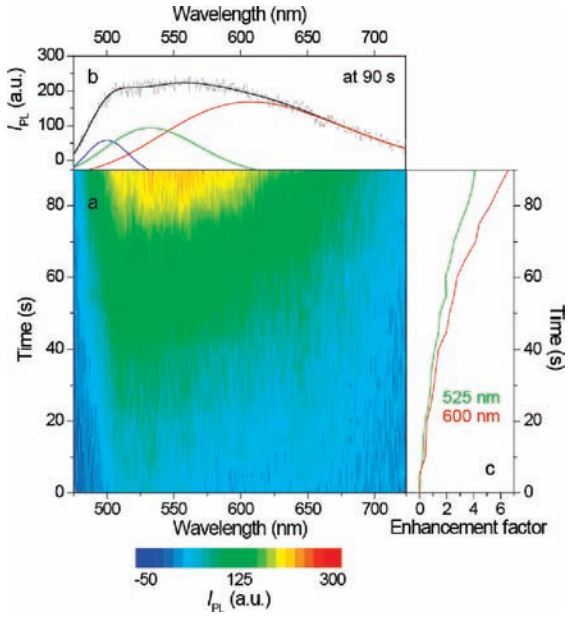

Figure 3. Time evolution of the PL spectra obtained during 405-nm laser excitation for a part of the single TNW under an Ar atmosphere (a). The spectra (b) and the enhancement factors (c), which are calculated by dividing the differential PL intensity by the original intensity, are shown in the upper and right sides, respectively. The solid lines in panel b indicate the Gaussian distributions fitted with the spectrum.

the time evolution of the PL spectra obtained during 405-nm laser excitation for a single TNW under an Ar atmosphere. The observed spectra are well reproduced by three Gaussian components centered at about 500 (2.48 eV, blue line), 533 (2.33 eV, green line), and 608 nm (2.04 eV, red line). By taking the spectral response of the detection system, particularly the effect of the cutoff filters, into account, the peak wavelength of the component with a highest energy should be shorter than 500 nm. In addition, the time evolution of the enhancement factors, which are calculated by dividing the differential PL intensity by the original intensity, indicates that the component around 600 nm increases more remarkably than that around 525 nm ($t > 40$ s). A similar spectral change was also observed for the single TiO_2 nanoparticles.[34]

Historically, the visible emission of TiO_2 is ascribed to the self-trapped excitons localized on the TiO_6 octahedra[58] or oxygen vacancies.[59] For instance, Sekiya et al. reported that the visible PL spectrum consists of three components centered at about 517, 577, and 636 nm, which are assigned to excitons bound to partially reduced Ti ions, self-trapped excitons through an exciton−lattice interaction, and oxygen vacancies, respectively.[60,61] Recently, McHale et al. observed the PL spectra of nanocrystalline TiO_2 in the anatase and rutile phases, and in mixed-phase samples at room temperature, and found that the total PL of anatase is a superposition of transitions involving spatially separated trapped electrons and holes.[62] In short, they suggested that the green PL with a peak around 525 nm is due

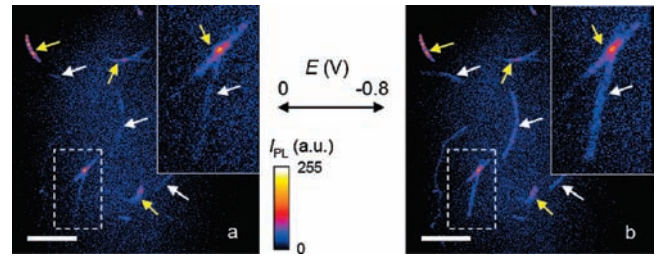

Figure 4. PL images of single TNWs acquired without (a) and with (b) applied potential (E) of −0.8 V vs Ag wire (= −0.37 V vs NHE). With the applied potential of −0.8 V, a significant increase in the PL intensity was observed. The activated and unactivated TNWs are indicated by the white and yellow arrows, respectively. Scale bars are 10 μm. Insets show expanded images of the areas enclosed by the broken lines.

to the transition between the mobile electrons (those in the conduction band or in shallow bulk traps) and trapped holes, and the red PL with a peak around 600 nm is due to that between the deeply trapped electrons and valence band holes. According to their assignment, our results indicate that at least two different light-emitting species due to the trapped charges are involved in the visible PL bands, and their distribution gradually changes during the photoirradiation.

In order to assign the trapped species, we measured the PL spectra of individual TNWs under 405-nm laser irradiation for 1 min in Ar-saturated EtOH. The result is given in Figure S9 (Supporting Information). The observed spectra with peaks at 520−540 nm resemble that reported in the literature.[62] The histogram for the intensity ratio of 525:610 nm also confirms the significant difference between spectra obtained in an Ar atmosphere and an Ar-saturated EtOH. On the basis of these results, it is inferred that the green PL of the TNW is partially attributed to the radiative recombination of mobile electrons and trapped holes.

Electric Potential-Induced PL. We applied the single-molecule spectroelectrochemical technique[35,36] to reveal the origin of the visible PL from individual TNWs. The cell configuration is described in the Experimental Section and illustrated in Figure S5 (Supporting Information). In a typical experiment, the potential of the working electrode, i.e., an indium tin oxide (ITO) thin film fabricated on a cover glass, was linearly scanned at a scan rate of 0.1 V s^{-1} with simultaneous measurement of the PL images of many single wires.

Figure 4B shows the PL images of single TNWs acquired without (a) and with (b) the applied potential (E) of −0.8 V vs Ag wire (= −0.37 V vs NHE). With the applied potential of −0.8 V, a noticeable increase in the PL intensity was observed. Note that no PL was detected at all without the 405-nm laser irradiation. In the images, the activated and unactivated TNWs are indicated by the white and yellow arrows, respectively. As depicted in the inset, the wire lying over another one on the ITO surface has a much lower response to the potential, indicating the importance of physical contact between the wire and ITO on the potential-induced PL and, moreover, the possibility that electron transport between physically contacted wires is inefficient. Additionally, one can distinguish the wires that have less contact with the ITO, because no significant PL quenching due to electron transfer from the photoexcited TiO_2 to the ITO was observed for these wires in the absence of the applied potential. This interpretation is supported by the fact that a remarkable suppression of the photoactivation was

(58) Tang, H.; Berger, H.; Schmid, P. E.; Levy, F.; Burri, G. *Solid State Commun.* **1993**, *87*, 847–850.
(59) Serpone, N.; Lawless, D.; Khairutdinov, R. *J. Phys. Chem.* **1995**, *99*, 16646–16654.
(60) Sekiya, T.; Kamei, S.; Kurita, S. *J. Lumin.* **2000**, *87*−*89*, 1140–1142.
(61) Sekiya, T.; Tasaki, M.; Wakabayashi, K.; Kurita, S. *J. Lumin.* **2004**, *108*, 69–73.
(62) Knorr, F. J.; Mercado, C. C.; McHale, J. L. *J. Phys. Chem. C* **2008**, *112*, 12786–12794.

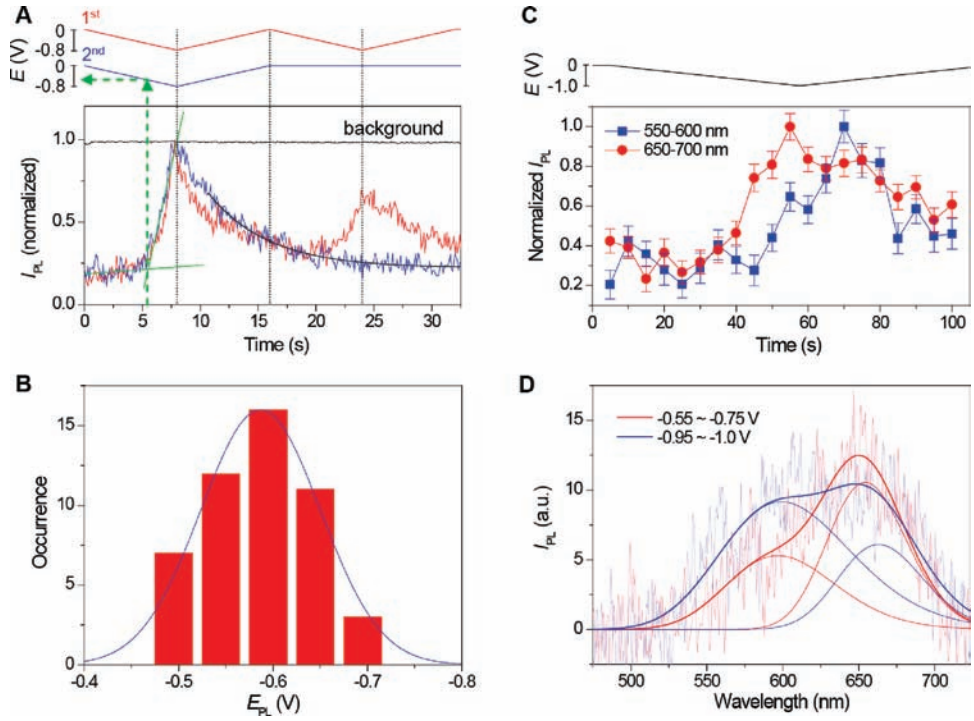

Figure 5. (A) Applied potential dependence of the normalized PL intensity obtained for the same position of identical TNWs. The green lines and arrows indicate the potential that begins to activate the PL (E_{PL}). The background signal is also shown. The dark gray line shows the single-exponential fit. (B) Histogram of E_{PL} determined for individual TNWs. The blue line indicates the Gaussian distribution fitted to the histogram. (C) Applied potential dependence of the normalized PL intensity obtained at 550−600 and 650−700 nm for the same position of identical TNWs. (D) PL spectra observed at different times. The solid lines indicate the Gaussian distributions fitted to the spectra.

observed for the TiO_2 nanoparticles on the ITO surface (Figure S10, Supporting Information).

Figure 5A represents the applied potential dependence of the normalized PL intensity obtained for identical TNWs. The first experiment (red), in which two potential cycles were applied, shows two peaks around $E = -0.8$ V, although the second peak is slightly weaker than the first one. The relative intensity of the first peak to the second one is 0.80 ± 0.15 for 20 individual TNWs. The second experiment (blue), in which the second potential cycle was applied after a 1-min intermission, also shows a peak with a fully recovered intensity at the same wire. It should be noted that the PL with several bursts gradually decays at the rate of 0.2 s^{-1}, which is about 3.5 times slower than the growth rate of PL during the application of a potential (see Movie S2, Supporting Information). Here, the potential that begins to activate the PL is defined as E_{PL} (see green lines in Figure 5A) and is determined for individual TNWs as shown in Figure 5B. The histogram of E_{PL} indicates a broad distribution with a peak around −0.6 V vs Ag wire (= −0.17 V vs NHE).

To assign the emissive transient species, we measured the PL spectra during the potential cycle between 0 and −1.0 V vs Ag wire at the scan rate of 0.02 V s^{-1}. These results are shown in Figure 5C. The blue squares and red circles show the potential dependence of the normalized PL intensity observed at 550−600 and 650−700 nm, respectively.[63] Interestingly, the PL intensity at 650−700 nm first began to increase more than that at 550−600 nm, where the E_{PL} values are estimated to be about −0.50 and −0.63 V vs Ag wire (= −0.07 and −0.20 V vs NHE) for the 650−700 and 550−600 nm regions, respectively. In addition, as shown in Figure 5D, the spectra are roughly divided into two components, i.e., those with a peaks around 600 and 660 nm. These results imply that several sites for electron trapping are included in the potential-induced PL process.[64]

Indeed, with the known potential-dependent adsorption and/or intercalation of cations to TiO_2, the material itself is expected to change as the Fermi energy is raised.[65] The flat band potentials have been estimated to be −1.2 to −1.1 V vs Ag wire (= −0.76 to −0.66 V vs NHE) in acetonitrile containing 0.1 M $LiClO_4$.[66,67] As is well known, numerous electron trap sites lie just below the conduction band. For a nanocrystalline TiO_2 electrode consisting of sintered anatase particles, the dependence of the charge accumulation rate constant on the initially applied potential has been used to infer the existence of an intraband state about 0.7 eV below the conduction band edge.[68] The subsequent spectroelectrochemical investigations of the nanocrystalline TiO_2 electrodes prepared from Degussa P25 (anatase (80%) and rutile (20%)) indicated the presence of

(63) We observed PL spectra of single TNWs immobilized on the cover glass in Ar-saturated 0.1 M $LiClO_4$ in acetonitrile similar to those observed under an Ar atmosphere (data not shown), suggesting that the PL spectra under the applied potential are not due to the solvent or electrolyte.

(64) The Gaussian distribution of the trap depths could be used instead of an exponential to account for the bias absorption spectra of the TiO_2 thin film.[65] However, as most of the studies assume an exponential trap-state distribution, we give the equivalent model for consistency as discussed below.

(65) Rothenberger, G.; Fitzmaurice, D.; Grätzel, M. *J. Phys. Chem.* **1992**, *96*, 5983–5986.
(66) Redmond, G.; Fitzmaurice, D. *J. Phys. Chem.* **1993**, *97*, 1426–1430.
(67) Staniszewski, A.; Morris, A. J.; Ito, T.; Meyer, G. J. *J. Phys. Chem. B* **2007**, *111*, 6822–6828.
(68) Redmond, G.; Fitzmaurice, D.; Grätzel, M. *J. Phys. Chem.* **1993**, *97*, 6951–6954.

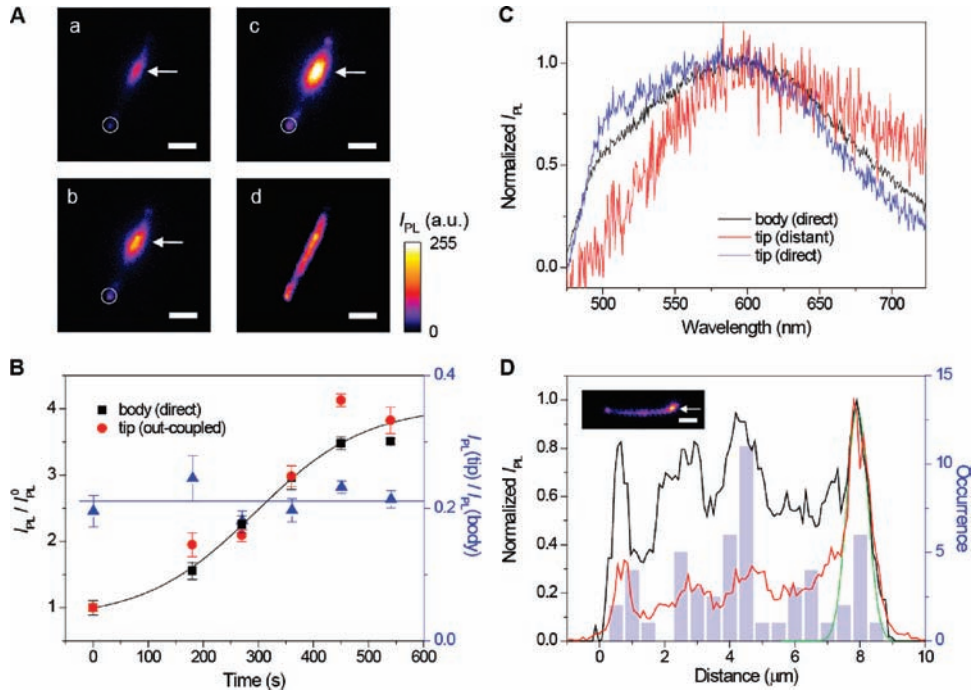

Figure 6. (A) PL images observed at 0 (a), 180 (b), and 360 s (c) during the 405-nm laser excitation of a single TNW. The white arrows indicate the irradiated area limited by a pinhole (diameter is ~1−2 μm on the cover glass). Scale bars are 2 μm. The PL image observed during laser irradiation of the whole area is also shown (d). (B) Time evolution of the relative PL intensity (I_{PL}/I^0_{PL}) acquired at the body (black) and tip (red). The ratio of the PL intensity at the tip to that at the body (I_{PL}(tip)/I_{PL}(body)) is also shown (blue). (C) PL spectra observed at the body (black) and tip (blue) of the wire, which are indicated by the white circle and arrow in image d of panel A, respectively, under direct 405-nm laser excitation in Ar. The spectrum of the out-coupled emission at the tip under distant excitation (see the arrow for the excitation position) is also shown (red). (D) Line profiles of the PL intensity under whole (black line) and local excitations (red line) and histogram of the number of counted bursts (light blue bars). The precise position at which a burst is generated is determined from Gaussian fits to the intensity profiles. The line profile of the irradiated area is indicated by the green line. Inset shows the PL image acquired under 405-nm laser excitation of the tip of the wire under an Ar atmosphere. The white arrow indicates the irradiated area limited by a pinhole. The scale bar is 2 μm.

traps at ~0.5 eV below the conduction band edge.[69] Similar studies of electrode films composed of small anatase particles showed that traps are present at ~0.5 eV below the conduction band edge.[70] In the present system, therefore, the energy level of trapped electrons is considered to be −0.5 to −0.7 V vs Ag wire (= −0.1 to −0.3 V vs NHE). This value is quite consistent with the E_{PL} values obtained by single-particle electrochemical spectral measurements. Thus, the electron transfer from free or shallowly trapped electrons to the ITO electrode (ca. 0 vs NHE)[71] is energetically possible, supporting the significant PL quenching of TNWs in contact with the ITO surface in the absence of the applied potential. On the other hand, the application of a negative potential results in the accumulation of (trapped) electrons in TiO_2. The observed slow PL decay implies the formation of deeply trapped electrons during application of the potential (Figure 5A). These electrons are stable until exposure to laser irradiation, during which photostimulated detrapping occurs to generate mobile electrons, followed by electron transfer to the ITO.

Local Excitation of Individual TNWs. As mentioned in the Introduction, the long-distance transport of charge carriers and the visible-light scattering enhanced in the nanostructured TiO_2 materials are key factors in the performance of devices such as DSSCs. In this section, we demonstrate that some individual TNWs can act as active waveguides where defect emissions propagate along the wire. One-dimensional optical waveguides consisting of semiconductors with high refractive indices, such as ZnO and SnO_2, are scientifically and technologically important for a wide variety applications including lasers, sensors, etc.[2,72] Furthermore, we found that the photogenerated color centers play an important role in remote PL, in which the spatially separated position can emit during laser excitation at distant positions.

Figure 6A shows the PL images observed during the 405-nm laser excitation of a single TNW. The irradiated area is limited by a pinhole (diameter is ~1−2 μm on the cover glass), as indicated by the white arrows. After several minutes of laser irradiation, in this case, a detectable emission emerged at the tip of the wire during laser irradiation (see circles in images a−c). Figure 6B also shows that the photoactivation of TNW PL at the body (black) is accompanied by a comparable increase in the emission intensity at the tip (red).

For a quantitative theoretical prediction of the waveguiding behavior,[57,73] the percent power (η) within the core of a step-index fiber in air is given by

$$\eta = 1 - \left(2.405 \exp\left[-\frac{1}{V}\right]\right)^2 V^{-3} \qquad (5)$$

where a and n are the width and the refractive index of the fiber, respectively, and $V = a\pi/\lambda(n^2 - 1)^{1/2}$. From the calcula-

(69) Boschloo, G. K.; Goossens, A. *J. Phys. Chem.* **1996**, *100*, 19489–19494.
(70) Boschloo, G.; Fitzmaurice, D. *J. Phys. Chem. B* **1999**, *103*, 2228–2231.
(71) Parker, I. D. *J. Appl. Phys.* **1994**, *75*, 1656–1666.
(72) Law, M.; Sirbuly, D. J.; Johnson, J. C.; Goldberger, J.; Saykally, R. J.; Yang, P. *Science* **2004**, *305*, 1269–1273.

tion, the waveguide ($a = 200$ nm and $n = 2.52$ (anatase TiO_2)[74]) for the 600-nm light contains ca. 80% of the power in the core (see Supporting Information for details concerning calculations of η, the number of possible modes (m), and the cutoff wavelength (λ_c), Figure S11). For the TNWs, however, it was found that only 20−30% of the wires with widely distributed a values (average value is ∼100 nm, Figure S2) behave as the active waveguide emitting light at the tip after the photoactivation process. This would be explained by the prediction that the η value significantly decreases with decreasing a (e.g., $\eta \approx$ 40% for the 100-nm waveguide).

Figure 6C represents the spatially resolved PL spectra acquired at different positions on the wire under 405-nm laser excitation. The PL spectrum at the tip exhibited a broad red emission with a peak around 600 nm (red), while the spectrum observed at the same position by the direct excitation (blue) is almost identical to that acquired at an excitation location on the body (black). This result indicates that the structures of the inherent defects on the wire differ only slightly at each position. In addition, the spectral measurements of the propagating light at the tip of the wire during photoirradiation of the body with a mercury lamp (100 W, Ushio, USH-102D) through a pinhole showed no significant attenuation in the waveguided emission with decreasing wavelength in the 500−600 nm range, indicating that the influence of reabsorption and Rayleigh scattering of the propagating light on the spectral shape is almost negligible (Figure S11, Supporting Information).

An investigation of the photoactivation process of TNW PL was next completed. Figure 6D shows the relationship between the intensity distribution of PL under local excitation (red line) and the photocatalytically active sites (blue bars), which are identified by observing the photon bursts during the overall excitation of the wire as already described, after the photoactivation process (black line). The green line indicates the line profile of the irradiated area. Interestingly, a close relationship between them was found for a number of wires (over 10 wires), implying that the photogenerated color centers play an important role in the remote PL at the distant positions on the wire.

We performed further experiments to prove that long-distance transport of charge carriers in the wire is involved in the remote PL process. This result is shown in Figure 7. First, a part of the wire body was irradiated for 30 min by 405-nm laser light through a pinhole to accumulate the deeply trapped electrons (i.e., color centers). The intensity profile of the PL acquired after sufficient photoactivation is indicated by the black line. Note that the waveguided emission was clearly observed at both tips of the wire (right image). When the irradiated spot was moved to a different position (left image and red line), a strongly enhanced emission was detected at the previously irradiated area (light blue). These results clearly demonstrate that the photoactivated area serves as the charge recombination center of the photogenerated charge carriers. To identify the origin of the emission, we measured the PL spectra from this area under both direct and distant excitations. As shown in Figure 7B, the PL spectrum observed for the distant excitation exhibited a relatively narrow red PL (red), as compared to a typical PL spectrum obtained by direct excitation of the photoactivated TNWs (black). The observed red PL is quite similar to that obtained under the applied negative potential, which was assigned to the

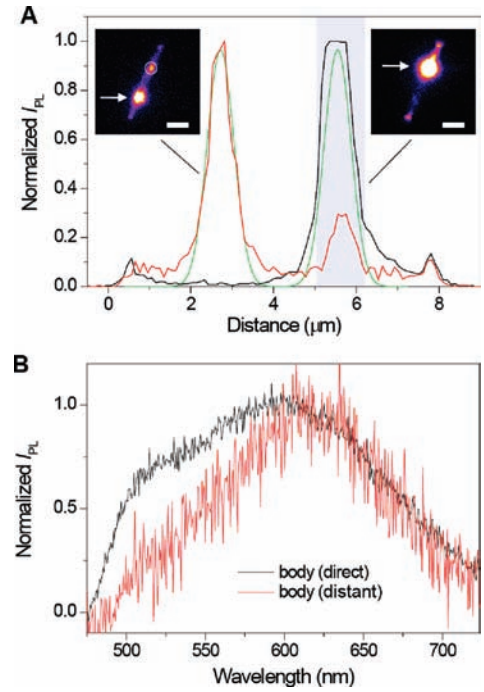

Figure 7. (A) Line profiles of the PL intensity under local excitation of the wire in Ar. The line profile of the irradiated area is shown in green. The white arrows in the images indicate the irradiated area limited by a pinhole. The black line was obtained after 405-nm laser irradiation of the body of the wire for 30 min (right image). The red line was obtained by changing the irradiated position after the photoactivation (left image). Scale bars are 2 μm. (B) PL spectra obtained at the body (see the white circle and the light blue area in panel A, respectively) of the wire during direct (black) and distant (red) excitations under an Ar atmosphere.

charge recombination between the deeply trapped electrons and mobile holes (Figure 5D). Thus, our findings imply that free (and shallowly trapped) charge carriers can migrate along the one-dimensional axis, but the deeply trapped ones on the surface cannot move efficiently.

Mechanism of Long-Distance Charge Transport in TNWs. A major research effort has been aimed at measuring the effective diffusion coefficient, D_n, and the effective lifetime, τ_n, in DSSCs under various conditions. These features have been addressed by using the multiple-trapping model,[75,76] the hopping model,[77,78] and the continuous time random walk model.[79,80] Based on the most frequently used multiple-trapping model, D_n describes the diffusion in a macroscopic concentration gradient under a quasiequilibrium condition.[21] D_n values ranging between 10^{-8} cm^2 s^{-1} at low light intensities and 10^{-4} cm^2 s^{-1} at high light intensities have been reported for the nanostructured TiO_2 thin-film electrode.[24,81,82] To obtain further information about

(73) Snyder, A. W.; Love, J. D. *Optical Waveguide Theory*; Chapman and Hall: London, 1983.
(74) Kingery, W. D.; Bowen, H. K.; Uhlmann, D. R. *Introduction to ceramics*, 2nd ed.; Wiley: New York, 1976.
(75) Tiedje, T.; Rose, A. *Solid State Commun.* **1981**, *37*, 49–52.
(76) Bisquert, J. *Phys. Rev. Lett.* **2003**, *91*, 010602/1–010602/4.
(77) Monroe, D. *Phys. Rev. Lett.* **1985**, *54*, 146–149.
(78) Bisquert, J. *J. Phys. Chem. C* **2007**, *111*, 17163–17168.
(79) Nelson, J. *Phys. Rev. B* **1999**, *59*, 15374–15380.
(80) Nelson, J.; Chandler, R. E. *Coord. Chem. Rev.* **2004**, *248*, 1181–1194.
(81) In contrast, the diffusion coefficients (D_0) of electrons and holes inside the nanocrystallites of anatase TiO_2 have been determined to be 0.01 and 0.4 cm^2 s^{-1}, respectively, which are several orders of magnitude higher than D_n.[82] This difference is due to the temporary immobilization of charges at the trapping sites and the intrinsic reduction in mobility due to path restrictions imposed by the porous geometry. Using D_0 and the diffusion length (L) of 3 μm (see Figure 7A), the transit times (τ_0) of electrons and holes in the wire are calculated to be 9 and 0.2 μs, respectively, on the basis of the carrier diffusion model: $\tau_0 = L^2/D_0$.

the charge carrier dynamics, we measured the transient absorption spectra and kinetic profiles of the photogenerated species, i.e., trapped electrons and holes, by nanosecond time-resolved diffuse reflectance (TDR) spectroscopy (Figure S12, Supporting Information). This result shows that the survival time of the trapped carriers is greater than 0.1 ms. Considering this lifetime and the D_n of 10^{-4} cm^2 s^{-1}, L_n is expected to reach a distance of a few micrometers.

We now propose a hypothetical model that explains the mechanism of the remote PL behavior. For the model, we assume that deeply trapped electrons are immobile, while electrons detrapped from the shallow trap sites located at the bottom of the conduction band are referred to as the mobile (conduction band) electrons. A similar assumption might be adopted for the holes in TiO_2.[83]

When the TNW is locally excited by 405-nm laser light, visible PL with a very broad spectrum is observed at the *corresponding* position due to charge recombination between the free and trapped carriers in the wire (Figures 6 and 7).[84] This is typical PL behavior. Meanwhile, some of the electrons migrate in the wire via a trapping-detrapping process and eventually reach the potential minima, i.e., deep trap sites, at the surface. These deep trap sites are visualized as luminescent active sites heterogeneously distributed over the material (Figures 1A and 2). The deeply trapped electrons, i.e., color centers, should absorb the guiding light, resulting in a much greater attenuation in the shorter wavelength region.[38,39] On the other hand, remote PL at the distant active sites, which is attributed to the radiative recombination between the deeply trapped electrons and mobile holes, emerges due to the carrier migration in the wire after a sufficient photoirradiation (Figure 6D). The dramatically enhanced red PL at the distant, *pre-irradiated* area, where a sufficient number of electrons could be stored, strongly supports the conclusion that the remote PL cannot be entirely explained by the wave-guiding effect (Figure 7).

Nevertheless, the question remains as to why the green PL was not detected at the distant position. It is not easy to address this question. One possible reason is a much longer lifetime of the trapped electrons in the wire than that of the trapped holes, which are consumed by water and/or hydroxyl groups on the surface.[18,85,86] Furthermore, the difference in the number of intrinsic defects should influence the efficiency of the carrier trapping. As shown in Figure S12 (Supporting Information), the TDR spectra showed that the generation yield of trapped electrons (holes) in the TNW is higher (lower) than that in the anatase TiO_2 nanoparticles (ST-01, Ishihara Sangyo). This result suggests that the number of electron (hole) trapping sites on the surface of the TNWs is much more (less) than that of the nanoparticles, and this well agrees with the finding that the synthetic TiO_2−B nanowires possess abundant surface states or oxygen vacancies as compared to the TiO_2 P25.[32]

In general, diffusion of electrons is faster than diffusion of holes in the nanocrystalline TiO_2, probably due to the lower activation energy for the electron transport.[26,27,87,88] However, it has been shown that the accumulation of trapped charges strongly influences the transport characteristics of the charge carriers in the semiconductor materials.[26,90] For instance, Duzhko et al. observed a change in the sign of the photovoltage for both anatase and rutile porous films under visible-light irradiation (wavelength, 442 nm) after subsequent exposure of the films to a vacuum.[26] They explained their observations by assuming that the diffusion coefficients of the charge carriers change from $D_h < D_e$ to $D_e < D_h$ due to the accumulation of trapped electrons. Recently, the importance of Coulomb repulsion between the surface-trapped and free electrons on their transport processes in single CdSe nanowires has been mentioned by Kuno et al.[91] A similar interaction between the surface-trapped and free holes (electrons) might accelerate the transport of mobile holes (electrons) in the TNWs. At this time, we believe that the process is more complicated since the accumulation of charges on the surface of the wire under photoirradiation would lead to a change in the carrier mobility as well as in the potential of the band edge.[92,93] The accumulation of trapped electrons or holes leads to a negative or positive shift of the potential of the conduction band edge, respectively. In our case, the key species are the trapped electrons according to the fact that only the red PL band was observed at the distant position (Figure 7B). Therefore, it is likely that the free holes in TNW favor migration to the electron-accumulated area which has a higher valence band potential. To accurately identify the underlying mechanism, however, further experimental and theoretical investigations are necessary.

Conclusions

In conclusion, we have shown the nature of visible PL from individual TiO_2−B nanowires (TNWs) using single-particle imaging techniques. Basically, the transition responsible for the TNWs' PL is similar to that of anatase TiO_2 nanoparticles and is assigned to the radiative recombination of the free and trapped charge carriers. Single-particle spectroelectrochemistry clearly revealed that the red PL around 600−650 nm is attributed to the deeply trapped electrons in the wire and the electron transport between physically contacted wires is inefficient. This information is useful not only for exploration but also for development of nanowire-based DSSCs and gives us a unique understanding not available from other methods.

From the single-molecule kinetic analysis of the bursts, we found that the quenching reaction of the color centers by oxygen

(82) Enright, B.; Fitzmaurice, D. *J. Phys. Chem.* **1996**, *100*, 1027–1035.
(83) Xie, Z.; Burlakov, V. M.; Henry, B. M.; Kirov, K. R.; Smith, H. E.; Grovenor, C. R. M.; Assender, H. E.; Briggs, G. A. D.; Kano, M.; Tsukahara, Y. *Phys. Rev. B* **2006**, *73*, 113317/1–113317/4.
(84) Considering that the thickness of the space-charge layer calculated for the TNW (ca. 50 nm) is comparable to the size of the wires (100 nm in width and 30 nm in height), a typical n-type semiconductor behavior in which electrons are accumulated in the bulk and holes are localized at the surface may account for the green PL observed during the initial stage of the photoactivation (Figure 3). See Supporting Information for calculation of the thickness of the space-charge layer.
(85) Tang, J.; Durrant, J. R.; Klug, D. R. *J. Am. Chem. Soc.* **2008**, *130*, 13885–13891.
(86) Bahnemann, D.; Henglein, A.; Lilie, J.; Spanhel, L. *J. Phys. Chem.* **1984**, *88*, 709–711.
(87) Deskins, N. A.; Dupuis, M. *J. Phys. Chem. C* **2008**, *113*, 346–358.
(88) According to the assumption that the green PL is originated from them,[51] another explanation is the short diffusion length of self-trapped excitons due to the strong electron−phonon interactions that give rise to polaron formation.[89]
(89) Hendry, E.; Wang, F.; Shan, J.; Heinz, T. F.; Bonn, M. *Phys. Rev. B* **2004**, *69*, 081101/1–081101/4.
(90) Kytin, V.; Petrov, A.; Timoshenko, V. Y.; Parkhutik, V.; Kashkarov, P. K.; Weidmann, J.; Koch, F.; Dittrich, T. *Phys. Status Solidi A* **2003**, *197*, 487–491.
(91) Protasenko, V.; Gordeyev, S.; Kuno, M. *J. Am. Chem. Soc.* **2007**, *129*, 13160–13171.
(92) Hagfeldt, A.; Bjoerksten, U.; Grätzel, M. *J. Phys. Chem.* **1996**, *100*, 8045–8048.
(93) Gregg, B. A.; Chen, S.-G.; Ferrere, S. *J. Phys. Chem. B* **2003**, *107*, 3019–3029.

follows a Langmuir−Hinshelwood mechanism. The dynamics of interfacial electron transfer from the color centers to adsorbed oxygen molecules on a millisecond time scale as presented here should limit the overall rate of the photocatalytic degradation of organic pollutants, as suggested elsewhere.[54,94] Moreover, the spatially resolved PL imaging techniques make it possible to ascertain the location of the luminescent active sites, which are roughly estimated to be 2−5 sites/μm of the wire. These active sites are closely related to structural disorders, which would inhibit the transport of charge carriers and the heterogeneous distribution of the surface states present in the individual wires, and are referred to as photocatalytically active sites that efficiently produce reactive oxygen species, such as $O_2^{\bullet-}$ and hydroxyl radical ($^{\bullet}$OH), during photoirradiation.[95]

We have successfully detected the remote PL from single TNWs in which the spatially separated positions can emit during laser excitation at distant positions. This observation is not fully explained by the well-established waveguiding effect. An appropriate interpretation for the long-distance charge transport in the wire is given in terms of the trapping−detrapping phenomena of the charge carriers. Our findings and methodologies have provided valuable insights into the mechanism of interfacial electron transfer from the trapped electrons to molecular oxygen as well as the spatial distribution and transport characteristics of charge carriers in TiO_2 nanomaterials with various morphologies.

Acknowledgment. The authors are grateful to Prof. Paul F. Barbara, Dr. John K. Grey, and members of the Center for Nano and Molecular Science and Technology (CNM) at the University of Texas at Austin for their hospitality and for their assistance with the single-molecule spectroelectrochemical technique used in this study. This work has been partly supported by a Grant-in-Aid for Scientific Research (Projects 17105005, 19750115, and others) from the Ministry of Education, Culture, Sports, Science and Technology (MEXT) of Japanese Government.

Supporting Information Available: Movies for the burst-like PL behavior and the electric potential-induced PL of TNWs (.avi files); estimation of the thickness of the space-charge layer of TNW; figures showing SEM (S1), TEM (S1), and AFM (S2) images, powder XRD pattern (S3), and steady-state UV−visible diffuse reflectance and emission spectra of TNWs (S4), cell configuration for single-particle electrochemical measurements (S5), PL images of TNWs before and after photoactivation (S6), "on" time probability density of the bursts (S7), quenching yield of the bursts (S8), PL spectra of TNWs in Ar-saturated EtOH (S9), photoactivation of TiO_2 nanoparticles on glass and ITO surfaces (S10), waveguiding properties of TNWs (S11), and TDR spectral measurements (S12). This material is available free of charge via the Internet at http://pubs.acs.org.

JA900194M

(94) Gerischer, H. *Electrochim. Acta* **1993**, *38*, 3–9.
(95) Naito, K.; Tachikawa, T.; Fujitsuka, M.; Majima, T. *J. Am. Chem. Soc.* **2009**, *131*, 934–936.